Ultra small Pd clusters in FER zeolite alleviate CO poisoning for effective low temperature carbon monoxide oxidation

Inhak Song,[a†‡] Iskra Z. Koleva,[b‡] Hristiyan A. Aleksandrov,[b*] Linxiao Chen,[a] Jaeyoung Heo[c], Dongsheng Li,[c] Yong Wang,[a,d] János Szanyi,[a*] and Konstantin Khivantsev[a*‡]

[a]Institute for Integrated Catalysis, Pacific Northwest National Laboratory, Richland, Washington 99352, United States

[b]Faculty of Chemistry and Pharmacy, Sofia University "St. Kliment Ohridski", 1, J. Bourchier boulevard, 1126 Sofia, Bulgaria

[c]Physical and Computational Sciences Directorate, Pacific Northwest National Laboratory, Richland, Washington 99352, United States

[d]Voiland School of Chemical Engineering and Bioengineering, Washington State University, Pullman, Washington 99164, United States

†(Present address) Graduate School of Energy and Environment (KU-KIST Green School), Korea University, Seoul 02841, Republic of Korea

[‡]These authors contributed equally

*Corresponding authors: HAA@chem.uni-sofia.bg, Janos.Szanyi@pnnl.gov, Konstantin.Khivantsev@pnnl.gov

ABSTRACT: Ultra small Pd_4 clusters form inside FER zeolite during low temperature treatment (100 °C) in the presence of humid CO gas. They effectively catalyze CO oxidation below 100°C, whereas Pd nanoparticles are not active as they are poisoned by CO. Using catalytic measurements, infrared (IR) spectroscopy, X-ray absorption spectroscopy (EXAFS), microscopy, and density functional theory calculations we provide the molecular level insight into this previously unreported phenomenon. Pd nanoparticles get covered with CO at low temperatures which effectively blocks O_2 activation until CO desorption occurs. Small Pd clusters in zeolites, in contrast, demonstrate fluxional behavior in the presence of CO, which significantly increases their affinity for binding O_2. Our study shows a pathway for achieving low temperature CO oxidation activity on the basis of well-defined Pd/zeolite system.

Introduction

Pd/zeolites are enigmatic model systems with unusual chemistry and relevance in the industry.[1-2] Entrapped metal ions or clusters with the steric constraints by the zeolite structure carry strong potential for various catalytic reactions.[3-4] The unusual state of the "naked" di/poly-valent metal ions in zeolites has recently been identified, providing framework for understanding high coordinative unsaturation and reactivity.[5-8]

These cations can be reduced to metallic Pd or Pt under certain reductive conditions, leading to rich chemistry and a smear of species present both in the micropores (smaller species) and outside zeolitic micropores (nanoparticles).[9-11,17-20] These metals are typically used for oxidative reactions of carbon monoxide, nitric oxide, and hydrocarbons. Carbon monoxide (CO) is a highly toxic pollutant gas that is produced by incomplete combustion of fossil fuels and is a major contributor to worsening air quality. Palladium (Pd) catalysts have been used for the oxidation of CO in various industrial applications due to their high activity.[17-23] However, the use of Pd catalysts can be expensive and may also suffer from issues such as deactivation and poisoning.[12] It is well-known for Pd nanoparticles that once CO adsorbs on them, O_2 dissociation sites are blocked (due to higher affinity of CO for Pd) and there is no activity in CO oxidation at low temperature.[13-14] Only when CO desorption begins to occur, do the nanoparticles start catalyzing CO oxidation. To overcome these limitations, we turn to zeolites as a support material for Pd catalysts. Zeolites are crystalline aluminosilicates with well-defined pore structures and high surface making them ideal candidates as supports. Herein, we show the simple way to prepare small Pd clusters in zeolite H-FER. Surprisingly, these clusters possess much higher reactivity than Pd particles. We utilize catalytic measurements, IR spectroscopy, EXAFS tools, and DFT calculations in order to unravel the molecular understanding of this previously unknown phenomenon. The results demonstrate the potential of Pd-zeolite catalysts for the efficient oxidation of CO, highlighting them as valuable candidates for various CO abatement applications.

Water enables reduction of Pd ions to Pd clusters by CO

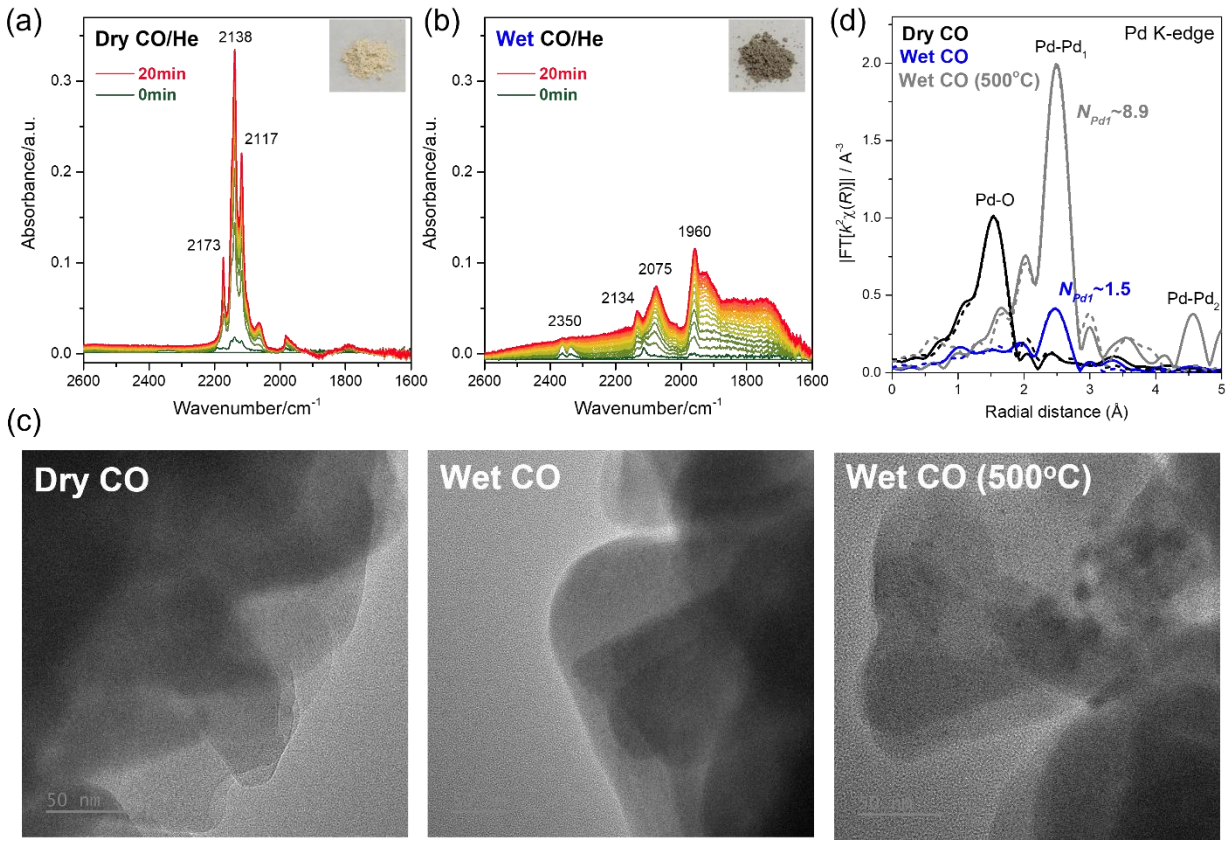

Figure 1. (a-b) Series of DRIFTS spectra (per 1 min) obtained at 100°C while flowing (a) 800ppm CO/He on dehydrated Pd/FER or (b) 800ppm CO+2.8% H_2O/He on hydrated Pd/FER. (c) Transmission electron microscopy (TEM) results on Pd/FER treated under dry and wet CO (100 and 500°C). (d) EXAFS in R-space magnitude over Pd/FER treated under various conditions (k^2-weighted, fittings shown as dashed curves of the same colors).

Pd-ion exchanged FER zeolite that used in this work was synthesized by incipient wetness impregnation method as described in our earlier works.[8, 10] The targeted amount of Pd was 1.8 wt.% and as-impregnated Pd/FER was calcined at 800 °C under ambient air for 5 h. More than 90% of Pd is present in an Pd(II) ion coordinated by zeolite framework after this high temperature treatment.[8] After *in situ* pretreatment of Pd/FER in DRIFTS cell at 500 °C under 3% O_2, cell was cooled down to 100 °C under He. Then, 800 ppm CO/He was introduced for 20 min (Figure 1a). Three sharp bands at 2173, 2138, and 2117 cm^{-1} rapidly appear with this dry CO adsorption. All these species are related to CO molecule coordinated to Pd(II) ion, either Pd(II)-CO or Pd(II)OH-CO, considering that there is almost no CO_2 formation during this dry CO adsorption (Figure S1). Interestingly, the presence of water totally changes the CO adsorption behavior for Pd/FER. For this wet CO adsorption, the sample was pre-oxidized under same condition and then saturated with water at 100 °C by flowing 2.8% H_2O for 30 min. After such hydration, 800 ppm CO was added to wet stream for 20 min (Figure 1b). Initially, the very small CO adsorbed on ionic Pd(II) at 2114 cm^{-1} was observed but rapidly disappeared. Then, the transient formation of gas phase CO_2 (2350 cm^{-1}) was clearly seen during initial few minutes exposure to CO, while linear CO (2075 cm^{-1}) and bridging CO (1960 cm^{-1}) adsorbed on metallic Pd gradually increase. New small band at 2134 cm^{-1} also simultaneously appears with the increase of CO band adsorbed on metallic Pd cluster. This feature can be assigned to CO adsorbed on Pd atoms covered with oxygen fragment, considering that this high wavenumber band is not observed in the experiments of CO adsorption on purely metallic Pd surface.[15] A large amount of CO consumption and CO_2 formation during wet CO adsorption was also monitored on mass spectrometer data (Figure S1). These observations undoubtedly show that Pd ions in FER zeolite are readily reduced to metallic Pd at 100 °C in the gas containing CO and H_2O together. The color of Pd/FER after exposure to dry and wet CO stream is also different (Inset in Figure 1a-b). The ionic Pd(II) dispersed in zeolite has a bright yellow color (dry CO), but turns to dark grey under wet CO. Interesting point is that we cannot observe any nanometer sized Pd particles after this wet CO treatment at 100 °C from microcopy (Figure 1c), which looks similar to sample image exposed to dry CO. This means that although Pd is reduced to metallic state under wet CO gas, its clustering is kinetically suppressed at mild temperature. We found that typical few nanometers sized Pd particles are formed only after high temperature exposure (Figure S2). EXAFS measurements were conducted to estimate the size of Pd clusters after *in situ* treatment in cell under various conditions (Figure 1d). Consistent with DRIFTS and TEM results, dry CO treatment does not lead to Pd reduction evidenced from dominant Pd-O scattering signal and the absence of Pd-Pd scattering. Typical high temperature CO reduction makes Pd-Pd_1 and Pd-Pd_2 scattering signal visible accompanied by disappearing Pd-O scattering, and our fitting results suggest the average coordination number of Pd (N_{Pd}) is ~8.9 (Figure 2, Table S1-2). This is consistent with the presence of few nanometers size Pd particles observed in above microcopy results. Interestingly, wet CO at 100 °C led to appearance of very small Pd-Pd_1 scattering while no Pd-Pd_2

scattering was observed. Calculated coordination number of Pd is ~1.5, meaning that this tiny Pd clusters inside FER zeolite contain less than 4-6 atoms based on mean particle size estimation.[16]

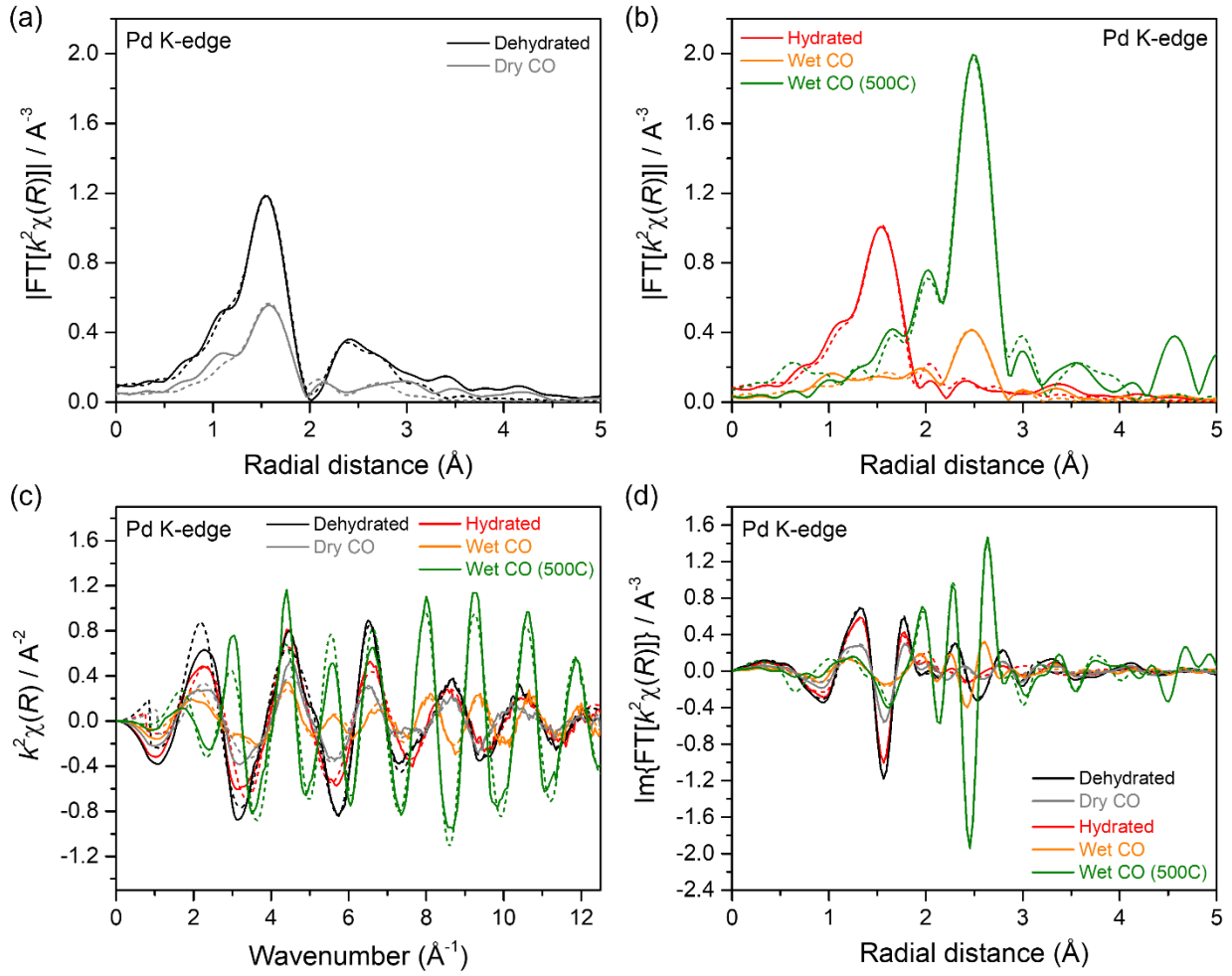

Figure 2. EXAFS data. (a-b) R-space magnitude over dehydrated or hydrated Pd/FER and their change under CO or CO+H_2O stream (k^2-weighted, fittings shown as dashed curves of the same colors). Panels (c) and (d) show the same data shown in (a-b), in *k*-space and *R*-space imaginary part, respectively. The spectra are color-coded in the same way, and fittings are shown as dashed curves of the same colors. This shows that the oscillation beyond 2.8 Å from Pd-Pd scattering beyond the first shell is negligible on the Pd/FER treated under wet CO at low temperature (100 °C).

Low temperature CO oxidation is facilitated by ultrasmall Pd clusters

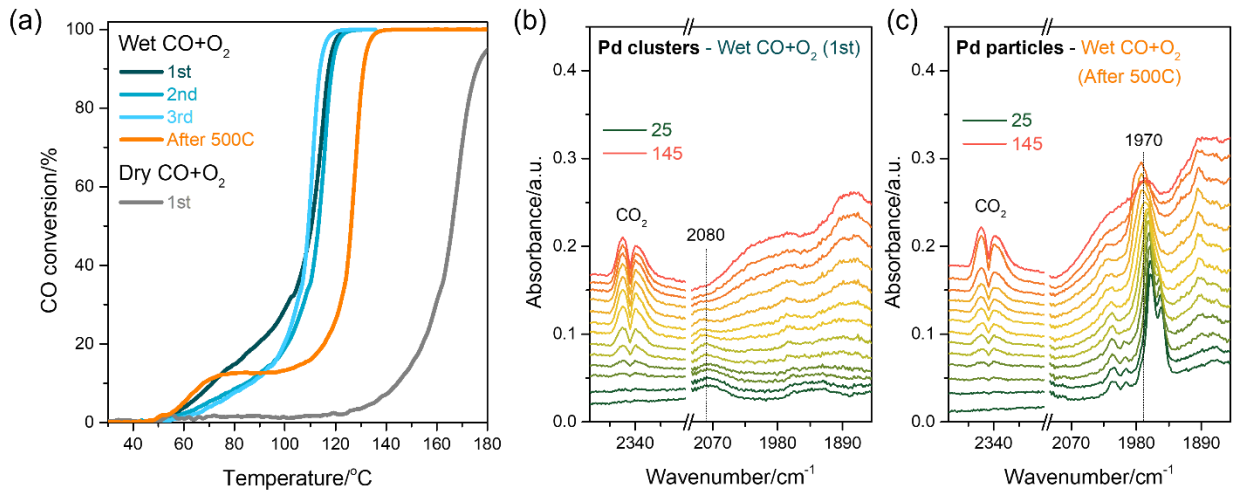

Figure 3. (a) Catalytic CO oxidation over Pd/FER catalyst in the presence and absence of water. For wet CO oxidation, light-off experiments were repeated three times from 25 to 135°C. After that, catalyst was exposed to 500°C for 30 min to make Pd nanoparticles and light-off experiment was conducted over this sample. The feed gas contains 1100ppm CO and 15% O_2 balance with N_2 (GHSV: 225,000 $mL \cdot g^{-1} \cdot h^{-1}$). (b-c) *In situ* DRIFTS spectra over Pd/FER during wet CO oxidation from 25 to 145°C (per 10°C) before and after forming Pd nanoparticles.

The results described above demonstrate that small Pd clusters inside FER zeolite can be synthesized with wet CO treatment at mild temperature. We compared the catalytic activity of this tiny Pd clusters with nanometer sized Pd nanoparticles for CO oxidation as model reaction. When Pd/FER was exposed to dry $CO+O_2$ stream, no CO oxidation activity was observed at low temperatures and CO oxidation did not begin to occur until above 125 °C (Figure 3a). It is because cationic Pd(II) in zeolite hardly dissociate oxygen molecules. Interestingly, CO start to be consumed only above 60 °C when Pd/FER was exposed to wet $CO+O_2$ stream. The activity increases rapidly around 100 °C and reaches 100% CO conversion below 125 °C. Such activity was repeatable during multiple reactions. A transient CO consumption between 50 and 100 °C that appears only for 1st reaction is due to the reduction of Pd(II) ions to small Pd clusters. Once Pd clusters are formed in zeolite, they can readily catalyze the CO oxidation at very low temperatures (<100 °C). Under steady state CO oxidation, this Pd clusters exhibit 85% conversion at 90 °C regardless of the presence of water (Figure S3). In contrast, Pd particles formed under high temperature reduction (Orange line in Figure 2a) exhibit less than 20% conversion until reaching 120 °C. *In situ* DRIFTS experiments were performed to observe surface species during CO oxidation at low temperatures (Figure 3b-c). For Pd clusters in zeolite, linear CO band (2080 cm^{-1}) on metallic Pd is observed to be dominant species. Although bridging CO band (1970 cm^{-1}) also appears with multiple CO oxidation cycle (Figure S4-5), its intensity is limited to certain extent. For Pd particles, however, bridging CO band (1970 cm^{-1}) is dominantly observed. It is noteworthy that CO band intensities on Pd particles is much larger compared to that on Pd clusters when exposed to same environment. Such markedly different CO coverage on Pd in the early stage of oxidation originate from size-dependent surface properties of metallic Pd clusters.

Modelling of CO and O_2 adsorption on Pd_{79} and Pd_4/FER models

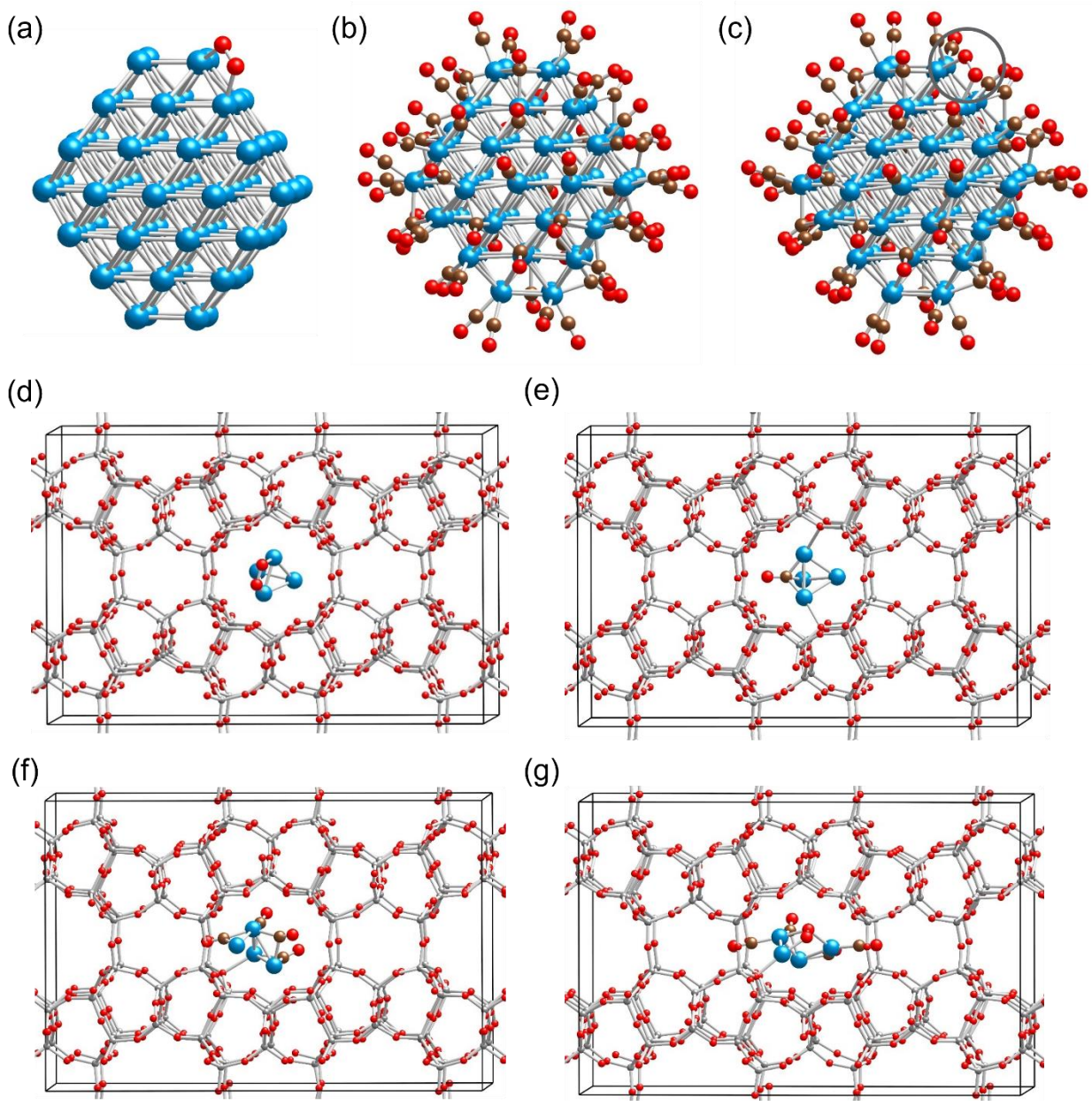

Figure 4. (a-c) Optimized models of $Pd_{79}(O_2)$, $Pd_{79}(CO)_{60}$ and $Pd_{79}(O_2)(CO)_{60}$. (d-g) Optimized models of $Pd_4(O_2)$/FER, $Pd_4(CO)$/FER, $Pd_4(CO)_4$/FER and $Pd_4(CO)_4(O_2)$/FER. Color coding: Si – gray; O – red; Pd – blue and C – brown. For visual clarity, the oxygen atoms from the CO molecules are represented with larger size.

Table 1. Binding energies of O_2, $BE(O_2)$, (in kJ/mol), number of unpaired electrons, N_s, and selected distances (in pm) for structures with O_2 and/or CO molecules adsorbed on Pd_{79} NP and Pd_4 cluster in Ferrierite cavity.

Structure	BE(O_2)	Ns	O-O	Δ(O-O)[a]	Pd-O
$Pd_{79}(O_2)$	-150	2	135.1	11.9	199;199
$Pd_4(O_2)$/FER	-164	2	134.7	11.5	204;205
$Pd_{79}(O_2)(CO)_{60}$	-107/-120[b]	0/2[b]	132.3/130.8[b]	9.1/7.6[b]	206;210/210;216[b]
$Pd_4(CO)_4(O_2)$/FER	-142	0	143.0	19.8	194;205;233

[a] Elongation of the O-O distance upon adsorption with respect to the bond length of an isolated in gas phase O_2 molecule, 123.2 pm; [b] spin-polarized system

The adsorption of sixty CO molecules on palladium nanoparticle, which consists of 79 atoms, was modelled (Figure 4a-c). We created the initial structure by saturating all the surface Pd atoms with CO molecules, i.e. one CO molecule is coordinated (top) to each Pd surface center. During the geometry optimization, some of the CO molecules moved from top to bridge or hollow coordination as consistent with experimental observation. Next, one oxygen molecule was adsorbed to the two Pd atoms which are most accessible for adsorbates and simultaneously with the lowest coordination. One of these atoms is located on the boundary between two (111) facets (edge of the nanoparticle), while another one is located at the corner between one of the (100) facets and two of the (111) facets. The binding energy of the oxygen molecule at this position is -107 kJ/mol and the O-O bond is elongated by 9.1 pm with respect to the bond length of an isolated in gas phase O_2 molecule (Table 1). The Pd-O distances are 206 and 210 pm. When the system was optimized in a spin-polarized fashion, the BE(O_2) is higher by 13 kJ/mol, but the elongation of the O-O bond is smaller – 7.6 pm and the Pd-O distances are slightly longer – 210 and 216 pm. In comparison, the binding energy of an oxygen molecule on pristine Pd_{79} nanoparticles (NP) is higher, -150 kJ/mol (Table 1). A model with a small Pd_4 cluster with a tetrahedron shape located in the larger channel of the zeolite Ferrierite was optimized. Interestingly, upon adsorption of four CO molecules (high CO coverage), a significant reconstruction of the Pd_4 cluster is observed and the tetrahedron shape is completely changed (Figure 4d-g). In order to check whether one CO molecule will cause a similar effect, we considered a structure in which one CO is adsorbed in a hollow position on the Pd_4 cluster, and in this case, the tetrahedron shape is preserved. The adsorption of CO molecules to Pd_4 cluster leads also to the shortening of the Pd-O_{zeo} bonds (Table S3). In the Pd_4/FER structure, the palladium cluster is located in the center of the zeolite cavity and is weakly bound to the oxygen centers from the Ferrierite as the average Pd-O_{zeo} distance is 284 pm while the shortest one is 266 pm. In $Pd_4(CO)$/FER and $Pd_4(CO)_4$/FER models the average distances are 265 and 271 pm, respectively, and the shortest ones are 246 and 242 pm, respectively (Table S3). After the adsorption of an oxygen molecule to the $Pd_4(CO)_4$ complex, the Pd-O_{zeo} distances are shortened further to an average value of 253 pm as the shortest distance is 226 pm. In this structure, the binding energy of the O_2 molecule, 142 kJ/mol, is higher by 35 kJ/mol compared to the case of $Pd_{79}(O_2)(CO)_{60}$ model, implying that the oxygen molecule binds stronger to the palladium cluster than to the palladium NP, most likely due to low coordinated metal centers occurring as a result of the strong relaxation of the cluster upon the adsorption of CO. The Pd_{79} NP is significantly larger and possesses a core of metal atoms inaccessible for CO adsorption which retains the shape of the nanoparticle and prevents significant relaxation of the nanoparticle structure upon adsorption of many CO molecules. A structure with palladium dimer located in the larger channel of the ferrierite was also optimized (Figure S6, Table S3). In the case of $Pd_2(CO)(O$-

$_2$)/FER and $Pd_2(CO)_2(O_2)$/FER models, the BE of oxygen is significantly lowered, resulting in very strong initial adsorption of CO. For example, the average BE of CO in the models $Pd_2(CO)$/FER and $Pd_2(CO)_2$/FER are as high as -394 and -274 kJ/mol, respectively, for comparison the corresponding values in the $Pd_4(CO)_4$/FER and $Pd_4(CO)_4(O_2)$/FER structures are -159 kJ/mol and -156 kJ/mol, respectively. Thus, Pd dimer is quite different from Pd_4 and strongly poisoned by CO, indicating that formation of a slightly larger (Pd_4) cluster confined in FER zeolite is key to activating oxygen at low temperatures.

Conclusions

Pd(II) cations in H-FER zeolite are resistant to carbon monoxide reduction under dry conditions. With the aid of FTIR, EXAFS, HRTEM characterization techniques and catalytic measurements we show that co-introduction of water with CO facilitates Pd(II) reduction with the formation of ultra-small metallic Pd clusters which catalyze low-temperature CO oxidation with much higher rate than isolated Pd(II) ions or Pd nanoparticles and which, unlike larger Pd particles, are not poisoned by CO. We explore the differences between small Pd clusters and Pd nanoparticles with theoretical calculations and reveal that the origin of this unusual low-temperature activity is the higher binding energy of oxygen molecule and more facile activation of O-O bond in the Pd_4 cluster with respect to the larger Pd clusters $\geq$ 1 nm in size.

Acknowledgments

The authors gratefully acknowledge the US Department of Energy (DOE), Energy Efficiency and Renewable Energy, Vehicle Technologies Office for the support of this work. The research described in this paper was performed in the Environmental Molecular Sciences Laboratory (EMSL), a national scientific user facility sponsored by the DOE's Office of Biological and Environmental Research and located at Pacific Northwest National Laboratory (PNNL). PNNL is operated for the US DOE by Battelle. IZK and HAA are grateful to the European Union-NextGenerationEU, through the National Recovery and Resilience Plan of the Republic of Bulgaria, project No BG-RRP-2.004-0008 for the financial support.

IZK and HAA also acknowledge the European Regional Development Fund within the Operational Programme "Science and Education for Smart Growth 2014–2020" under the Project CoE "National center of mechatronics and clean technologies" BG05M2OP001-1.001-0008 for the provided computational resources.

References

1. Djakovitch, L.; Koehler, K., Heck Reaction Catalyzed by Pd-Modified Zeolites, *Journal of the American Chemical Society* **2001,** 123 (25), 5990-5999.
2. Petrov, A. W.; Ferri, D.; Krumeich, F.; Nachtegaal, M.; van Bokhoven, J. A.; Kröcher, O., Stable complete methane oxidation over palladium based zeolite catalysts, *Nature communications* **2018,** 9 (1), 2545.
3. Cui, T. L.; Ke, W. Y.; Zhang, W. B.; Wang, H. H.; Li, X. H.; Chen, J. S., Encapsulating Palladium Nanoparticles Inside Mesoporous MFI Zeolite Nanocrystals for Shape-Selective Catalysis, *Angewandte Chemie* **2016,** 128 (32), 9324-9328.
4. Miriam Navlani-García, Izaskun Miguel-García, Ángel Berenguer-Murcia, Dolores Lozano-Castelló, Diego Cazorla-Amorós, Hiromi Yamashita, Pd/zeolite-based catalysts for the preferential CO oxidation reaction: ion-exchange, Si/Al and structure effect, *Catal. Sci. Technol.,* 2016, 6, 2623-2632.
5. Khivantsev, K.; Jaegers, N. R.; Koleva, I. Z.; Aleksandrov, H. A.; Kovarik, L.; Engelhard, M.; Gao, F.; Wang, Y.; Vayssilov, G. N.; Szanyi, J., Stabilization of Super Electrophilic Pd+2 Cations in Small-Pore SSZ-13 Zeolite, *The Journal of Physical Chemistry C* **2019,** 124 (1), 309-321.
6. Khivantsev, K.; Jaegers, N. R.; Kovarik, L.; Hanson, J. C.; Tao, F.; Tang, Y.; Zhang, X.; Koleva, I. Z.; Aleksandrov, H. A.; Vayssilov, G. N., Szanyi, J. Achieving Atomic Dispersion of Highly Loaded Transition Metals in Small-Pore Zeolite SSZ-13: High-Capacity and High-Efficiency Low-Temperature CO and Passive NOx Adsorbers, *Angewandte Chemie International Edition* **2018,** 57 (51), 16672-16677.
7. Khivantsev, K.; Wei, X.; Kovarik, L.; Jaegers, N. R.; Walter, E. D.; Tran, P.; Wang, Y.; Szanyi, J., alladium/Ferrierite versus Palladium/SSZ-13 Passive NOx Adsorbers: Adsorbate-Controlled Location of Atomically Dispersed Palladium(II) in Ferrierite Determines High Activity and Stability, *Angewandte Chemie* **2022,** 134 (3), e202107554.
8. Song, I.; Khivantsev, K.; Wu, Y.; Bowden, M.; Wang, Y.; Szanyi, J. Unusual water-assisted NO adsorption over Pd/FER calcined at high temperatures: The effect of cation migration, *Applied Catalysis B: Environmental* **2022,** 318, 121810.
9. Cheng, K.; Smulders, L. C.; van der Wal, L. I.; Oenema, J.; Meeldijk, J. D.; Visser, N. L.; Sunley, G.; Roberts, T.; Xu, Z.; Doskocil, E., Maximizing noble metal utilization in solid catalysts by control of nanoparticle location, *Science* **2022,** 377 (6602), 204-208.
10. Song, I.; Khivantsev, K.; Wang, Y.; Szanyi, J., Elucidating the Role of CO in the NO Storage Mechanism on Pd/SSZ-13 with in Situ DRIFTS, *The Journal of Physical Chemistry C* **2022,** 126 (3), 1439-1449.
11. Ma, Y.; Song, S.; Liu, C.; Liu, L.; Zhang, L.; Zhao, Y.; Wang, X.; Xu, H.; Guan, Y.; Jiang, J., Germanium-enriched double-four-membered-ring units inducing zeolite-confined subnanometric Pt clusters for efficient propane dehydrogenation, *Nature Catalysis* **2023**, 1-13.
12. Jiang, D.; Khivantsev, K.; Wang, Y., Low-Temperature Methane Oxidation for Efficient Emission Control in Natural Gas Vehicles: Pd and Beyond, *ACS Catalysis* **2020,** 10 (23), 14304-14314.
13. Darby, M. T.; Sykes, E. C. H.; Michaelides, A.; Stamatakis, M., Carbon Monoxide Poisoning Resistance and Structural Stability of Single Atom Alloys, *Topics in catalysis* **2018,** 61 (5-6), 428-438.
14. Hoffmann, J.; Meusel, I.; Hartmann, J.; Libuda, J.; Freund, H.-J., Reaction Kinetics on Heterogeneous Model Catalysts: The CO Oxidation on Alumina-Supported Pd Particles, *Journal of Catalysis* **2001,** 204 (2), 378-392.
15. Ozensoy, E.; Goodman, D. W., Vibrational spectroscopic studies on CO adsorption, NO adsorption CO þ NO reaction on Pd model catalysts, *Physical Chemistry Chemical Physics* **2004,** 6 (14), 3765-3778.
16. Jentys, A., Estimation of mean size and shape of small metal particles by EXAFS, *Physical Chemistry Chemical Physics* **1999,** 1 (17), 4059-4063.

17. C. Hess, E. Ozensoy, D. W. Goodman, Combined in Situ Infrared and Kinetic Study of the Catalytic CO + NO Reaction on Pd(111) at Pressures up to 240 mbar, J. Phys. Chem. B 2003, 107, 12, 2759–2764

18. Z. Say, M. Kaya, C. Kaderoğlu, Y. Koçak, K. Emre Ercan, A. Tetteh Sika-Nartey, A. Jalal, A. Arda Turk, C. Langhammer, M. Jahangirzadeh Varjovi, E. Durgun, E. Ozensoy, Unraveling Molecular Fingerprints of Catalytic Sulfur Poisoning at the Nanometer Scale with Near-Field Infrared Spectroscopy, *J. Am. Chem. Soc.* 2022, 144, 19, 8848–8860.

19. B. Song, S. Si, A. Soleymani, Y. Xin, H. E. Hagelin-Weaver, Effect of ceria surface facet on stability and reactivity of isolated platinum atoms, Nano Research 2022 https://doi.org/10.1007/s12274-022-4251-4.

20. B. Song, D. Choi, Y. Xin, C. R. Bowers, H. Hagelin-Weaver, Ultra-Low Loading Pt/CeO2 Catalysts: Ceria Facet Effect Affords Improved Pairwise Selectivity for Parahydrogen Enhanced NMR, *Angew. Chem. Int. Edit.* 2021, 60, 4038-4042.

21. Oh, D.G.; Aleksandrov, H.A.; Kim, H.; Koleva, I.Z.; Khivantsev, K.; Vayssilov, G.N.; Kwak, J.H. Understanding of Active Sites and Interconversion of Pd and PdO during CH4 Oxidation. Molecules **2023**, 28, 1957. https://doi.org/10.3390/molecules28041957

22. I. Z. Koleva, H. A. Aleksandrov, G. N. Vayssilov, Comparison of the Reactivity of Platinum Cations and Clusters Supported on Ceria or Alumina in Carbon Monoxide Oxidation, ACS Catal. 2023, 13, 8, 5358–5374

23. Oh, D. G.; Aleksandrov, H. A.; Kim, H.; Koleva, I. Z.; Khivantsev, K.; Vayssilov, G. N.; Kwak, J. H. Key Role of a-Top CO on Terrace Sites of Metallic Pd Clusters for CO Oxidation. *Chem. – Eur. J.* **2022**, *28*, e202200684, DOI: 10.1002/chem.202200684

Supplementary Information for

Ultra small Pd clusters in FER zeolite alleviate CO poisoning for effective low temperature carbon monoxide oxidation

Inhak Song,[a†‡] Iskra Z. Koleva,[b‡] Hristiyan A. Aleksandrov,[b]* Linxiao Chen,[a] Jaeyoung Heo[c], Dongsheng Li,[c] Yong Wang,[a,d] János Szanyi,[a]* and Konstantin Khivantsev[a]*[‡]

[a]Institute for Integrated Catalysis, Pacific Northwest National Laboratory, Richland, Washington 99352, United States

[b]Faculty of Chemistry and Pharmacy, Sofia University "St. Kliment Ohridski", 1, J. Bourchier boulevard, 1126 Sofia, Bulgaria

[c]Physical and Computational Sciences Directorate, Pacific Northwest National Laboratory, Richland, Washington 99352, United States

[d]Voiland School of Chemical Engineering and Bioengineering, Washington State University, Pullman, Washington 99164, United States

†(Present address) Graduate School of Energy and Environment (KU-KIST Green School), Korea University, Seoul 02841, Republic of Korea

[‡]These authors contributed equally

*Corresponding authors: HAA@chem.uni-sofia.bg, Janos.Szanyi@pnnl.gov, Konstantin.Khivantsev@pnnl.gov

Experimental methods

List of supplementary Tables and Figures

Table S1. Fitting parameters from the best EXAFS models of Pd/FER zeolite under dry condition.

Table S2. Fitting parameters from the best EXAFS models of Pd/FER zeolite and Pd foil under wet condition.

Table S3. Binding energies of O_2, BE(O_2), (in kJ/mol), number of unpaired electrons, N_s, and selected distances (in pm) for structures with O_2 and/or CO molecules adsorbed to Pd_{79} NP as well as Pd_2 and Pd_4 clusters located in pores of Ferrierite. Bader charges (in |e|) of the Pd atoms in the Pd clusters supported in FER are also shown.

Figure S1. (a-b) Series of DRIFTS spectra (per 1 min) obtained at 100 °C while flowing (a) 800 ppm CO/He on dehydrated Pd/FER or (b) 800 ppm CO+2.8% H_2O/He on hydrated Pd/FER. Different intensities of T-O-T vibration are due to hydration of Pd^{2+} cations in the presence of water. (c) CO and CO_2 profiles from mass spectrometer at the rear end of DRIFTS cell during dry and wet CO treatment.

Figure S2. Extra transmission electron microscopy (TEM) results on Pd/FER treated under dry and wet CO (100 and 500 °C).

Figure S3. (a) Effect of temperature and (b) effect of water on catalytic CO oxidation over wet CO treated (125 °C, 30min) Pd/FER catalyst. The feed gas contains 1100 ppm CO and 15% O_2 balance with N_2 (GHSV: 225,000 $mL \cdot g^{-1} \cdot h^{-1}$).

Figure S4. *In situ* DRIFTS spectra over Pd/FER during 2nd and 3rd wet CO oxidation from 25 to 125 °C (per 10°C, as in Figure 2). These experiments were conducted after conducting 1st CO oxidation in Figure 2b.

Figure S5. Series of DRIFTS spectra (per 1 min) obtained at 100 °C while flowing 800 ppm CO+15% O_2+2.8% H_2O/He on hydrated Pd/FER.

Figure S6. Left to right, top to bottom – optimized models of Pd_2/FER, $Pd_2(O_2)$/FER, $Pd_2(CO)$/FER, $Pd_2(CO)(O_2)$/FER, $Pd_2(CO)_2$/FER, $Pd_2(CO)_2(O_2)$/FER_1, $Pd_2(CO)_2(O_2)$/FER_2 and $Pd_2(CO)_2(O)_2$/FER. Color coding: Si – gray; O – red; Pd – blue and C – brown. For visual clarity, the oxygen atoms from the CO molecules are represented with larger size and structures $Pd_2(CO)_2$/FER, $Pd_2(CO)_2(O_2)$/FER_1, $Pd_2(CO)_2(O_2)$/FER_2 and $Pd_2(CO)_2(O)_2$/ FER are rotated by 90º with respect to the others.

Figure S7. Radial distribution function for the Pd-Pd distances in the pristine and covered by CO Pd_4/FER and Pd_{79} nanoparticle models.

Experimental methods

Pd ion exchanged ferrierite-type zeolite (Pd/FER) with 1.8 wt.% Pd loading were made by typical incipient wetness impregnation method. Normally, commercial NH_4-form FER-type zeolite with Si:Al~10 was purchased from Zeolyst, and 10 wt.% tetraamine palladium(II) nitrate solution in H_2O (Sigma Aldrich) was used for preparation. About 1 g of NH_4-FER powder was dried in an oven at 70°C for 1 h before impregnation. Then, targeted amount of palladium precursor solution was slowly added, i.e. 10μL at once by using pipet, to NH_4-FER powder while doing continuous mixing and grinding. The resulting white powder was dried in an oven at 70 °C overnight, and subsequently calcined in air at 800 °C for 5 h with the ramping rate of 2 °C/min. The color of Pd/FER powder becomes bright yellow after high-temperature treatment. The synthesized Pd/FER samples were stored in vials under ambient conditions.

The CO oxidation reaction test was performed using a plug flow reactor system where the concentrations of reactants and products are quantified using a FTIR gas analyzer (MKS, Multigas 2030). The catalyst powders were loaded in a quartz reactor above a porous bed. The temperature programed reactions were performed under 1100 ppm CO, 2.5% H_2O (when used), and 15% O_2/N_2 by ramping the reactor with 5 °C/min (GHSV: 225,000 $mL \cdot g^{-1} \cdot h^{-1}$).

The *in situ* diffuse reflectance IR measurements were performed in a commercial DRIFTS cell with ZnSe window. The spectra were collected on Nicolet iS50 FT-IR (Thermo Fisher Scientific Co., USA) spectrometer equipped with a liquid nitrogen-cooled MCT detector, and each spectrum was collected as the average of 32 scans with 4 cm^{-1} resolution. A background spectrum was obtained with KBr powder at temperatures where measurements were conducted. The space through which the IR beam passes on both sides of the reactor window was continuously purged with nitrogen to maintain a constant background. The sample cup inside DRIFTS cell was filled with α-alumina powder in a typical experiment. The α-alumina powder was confirmed to be inert under experimental conditions. A 0.025g of Pd/FER powder was spread over α-alumina powder and pressed firmly. Gas stream through the DRIFTS cell was controlled by mass flow controllers. Moisture was added by flowing the gas through a glass bubbler filled with distilled water at room temperature. The flow rate was adjusted to 50 mL/min (GHSV~120,000 $mL \cdot g^{-1} \cdot h^{-1}$). The outlet of the DRIFTS cell was connected to a quadrupole mass spectrometer (Hiden Analytical).

To investigate the difference between samples, we acquired HRTEM images. For the sample preparation, all powder samples were re-dispersed in ethanol, and ~ 10 μl of the solutions were dropcasted to TEM grids. With the sample grids, HRTEM images were collected with a Tecnai F20 TEM microscope (Thermofisher, USA) operated at 200 kV.

We employed DFT-D2 periodic calculations using PBE functional and D2 Grimme's dispersion correction. The Brillouin zone is sampled using only the Gamma point and the cut-off of the planewave basis set is 700 eV. The geometry relaxation was performed until all forces acting on the atoms became lower than 0.02 eV/Å. The Ferrierite structure model has the following cell parameters: a = 28.609 Å, b = 15.075 Å, c = 18.988 Å, α = β = γ = 90°, and the unit cell contains $Si_{144}O_{288}$. For the Pd_{79} NP was used a unit cell with the following parameters: a = b = c = 20.000 Å, α = β = γ = 90°.

Table S1. Fitting parameters from the best EXAFS models of Pd/FER zeolite under dry condition.

		Pd foil	Pd/FER	
			Dehydrated (20% O_2, pretreated at 500°C)	**Dry CO (2000 ppm CO/He after dehydration)**
***k*-range**		3-12.5	3-12.5	3-12.5
***R*-range**		1-3.9	1-2.9	1-2.9
***R*-factor**		0.0061	0.0041	0.0296
S_0^2		0.80 (4)	0.8	
ΔE_0		-3.0 (4)	3 (2)	4 (3)
O_1	***N***	N/A	4.3 (4)	1.9 (4)
	***R* (Å)**		2.02 (1)	2.04 (2)
	σ^2		0.003 (1)	0.003 (2)
Pd_1	***N***	12	N/A	N/A
	***R* (Å)**	2.741 (2)		
	σ^2	0.0054 (3)		
Si_1 (Non-bonding)	***N***	N/A	7 (3)	1 (1)
	***R* (Å)**		2.84 (2)	2.91 (4)
	σ^2		0.018 (6)	0.007 (12)
O_2 (Non-bonding)	***N***		4 (2)	1.3 (1)
	***R* (Å)**		3.42 (3)	3.42 (7)
	σ^2		0.003 (1)	0.003 (2)

S_o^2 was determined from the most appropriate fitting of Pd foil data. ΔE_o was set identical for all paths in each sample. Numbers in parentheses represent standard deviations of the last digit, while parameters without standard deviations were set to reasonable values. Pd foil was measured at 25 °C as a reference between ion chambers, while all Pd/FER spectra were measured inside an *in-situ* reactor at 100°C.

Table S2. Fitting parameters from the best EXAFS models of Pd/FER zeolite and Pd foil under wet condition.

		Pd foil	Pd/FER		
			Hydrated (2.5% H_2O/He) - 100°C	**Wet CO (2000 ppm CO+2.5% H_2O/He) - 100°C**	**Wet CO (2000 ppm CO+2.5% H_2O/He) - 500°C**
***k*-range**		3-12.5	3-12.5	3-12.5	3-12.5
***R*-range**		1-3.9	1-2.0	1-3.9	1-3.9
***R*-factor**		0.0061	0.0065	0.0368	0.0125
S_0^2		0.80 (4)	0.80		
ΔE_0		-3.0 (4)	2 (1)	0 (1)	-3.2 (7)
O	***N***	N/A	3.0 (3)	0.7 (2)	0.2 (2)
	***R* (Å)**		2.02 (1)	1.99 (3)	1.13 (20)
	σ^2		0.002 (1)	0.042 (17)	0.006
Pd_1	***N***	12	N/A	1.5 (3)	8.9 (7)
	***R* (Å)**	2.741 (2)		2.718 (7)	2.737 (4)
	σ^2	0.0054 (3)		0.0058 (9)	0.0068 (5)
Pd_2	***N***	6	N/A	N/A	5 (5)
	***R* (Å)**	3.89 (1)			3.89 (3)
	σ^2	0.009 (1)			0.014 (7)
Pd_1-Pd_1	***N***	48	N/A	1.1 (1)	40 (3)
	***R* (Å)**	4.13		4.067 (15)	4.106 (6)
	σ^2	0.0082 (4)		0.015	0.015

S_o^2 was determined from the most appropriate fitting of Pd foil data. ΔE_o was set identical for all paths in each sample.
Numbers in parentheses represent standard deviations of the last digit, while parameters without standard deviations were set to reasonable values.
Pd foil was measured at 25 °C as a reference between ion chambers, while all Pd/FER spectra were measured inside an *in-situ* reactor at 100°C.

Table S3. Binding energies of O_2, BE(O_2), (in kJ/mol), number of unpaired electrons, N_s, and selected distances (in pm) for structures with O_2 and/or CO molecules adsorbed to Pd_{79} NP as well as Pd_2 and Pd_4 clusters located in pores of Ferrierite. Bader charges (in |e|) of the Pd atoms in the Pd clusters supported in FER are also shown.

Structure	BE(O_2)	Ns	O-O	Δ(O-O)[a]	Pd-O	Pd-O_{zeo}/Average Pd-O_{zeo}	Pd-Pd/Average Pd-Pd	Bader charge Pd
$Pd_{79}(O_2)$	-150	2	135.1	11.9	199;199	–	275 – average value obtained from radial distribution function	–
$Pd_{79}(O_2)(CO)_{60}$	-107/ -120[e]	0/2	132.3/ 130.8[e]	9.1/7.6[e]	206;210/210;216	–	275 – average value obtained from radial distribution function	–
Pd_2/FER	–	0	–	–	–	273;289/281	260/260	0.03;0.04
$Pd_2(O_2)$/FER	-259	0	142.0	18.8	195;197	229;236/233	252/252	0.34;0.36
$Pd_2(CO)$/FER[b]	–	0	–	–	–	249;252/251	265/265	0.12;0.13
$Pd_2(CO)(O_2)$/FER[b]	-41	2	130.4	7.2	224;224	260;288/274	257/257	0.37;0.38
$Pd_2(CO)_2$/FER[c]	–	0	–	–	–	267;268/268	265/265	0.15;0.22
$Pd_2(CO)_2(O_2)$/FER_1[d]	-36	0	139.3	16.1	197;200	240/240	266/266	0.34;0.54
$Pd_2(CO)_2(O_2)$/FER_2[d]	-33	0	144.6	21.4	203;204;220;222	267;285/276	398/398	0.54;0.54
$Pd_2(CO)_2(O)_2$/FER[d]	-84	0	253.2	130.0	194;197;199;200	234/234	302/302	0.77;0.77
Pd_4/FER	–	0	–	–	–	266;282;283;294;296/284	259;260;261;262;265;265/262	0.01;0.02;0.02;0.04
$Pd_4(O_2)$/FER	-164	2	134.7	11.5	204;205	249;250/250	243;252;268;269;273;275/263	-0.03;0.02;0.31;0.31
$Pd_4(CO)$/FER	–	0	–	–	–	246;250;280;285/265	269;270;271; 277;281;282/275	-0.08;0.11;0.16;0.17
$Pd_4(CO)_4$/FER	–	0	–	–	–	242;272;283;287/271	260;273;276;288/274	0.14;0.26;0.26;0.27
$Pd_4(CO)_4(O_2)$/FER	-142	0	143.0	19.8	194;205;233	226;251;281/253	256;262;274/264	0.25;0.35;0.36;0.43

[a] Elongation of the O-O distance upon adsorption with respect to the bond length of an isolated in gas phase O_2 molecule, 123.2 pm; [b] The CO molecule is coordinated to two Pd atoms (bridge coordination); [c] One CO molecule is linearly coordinated, the other one is in bridge position; [d] Both CO molecules are coordinated to one Pd atom (linear coordination); [e] spin-polarized system

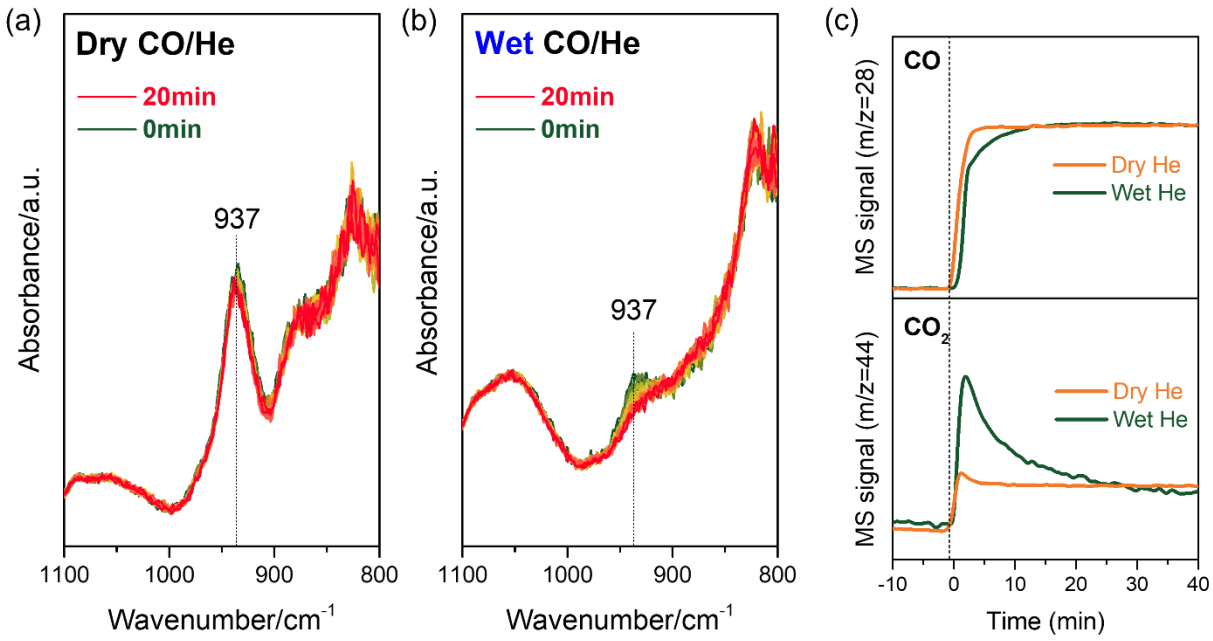

Figure S1. (a-b) Series of DRIFTS spectra (per 1 min) obtained at 100 °C while flowing (a) 800 ppm CO/He on dehydrated Pd/FER or (b) 800 ppm CO+2.8% H_2O/He on hydrated Pd/FER. Different intensities of T-O-T vibration are due to hydration of Pd^{2+} cations in the presence of water. (c) CO and CO_2 profiles from mass spectrometer at the rear end of DRIFTS cell during dry and wet CO treatment.

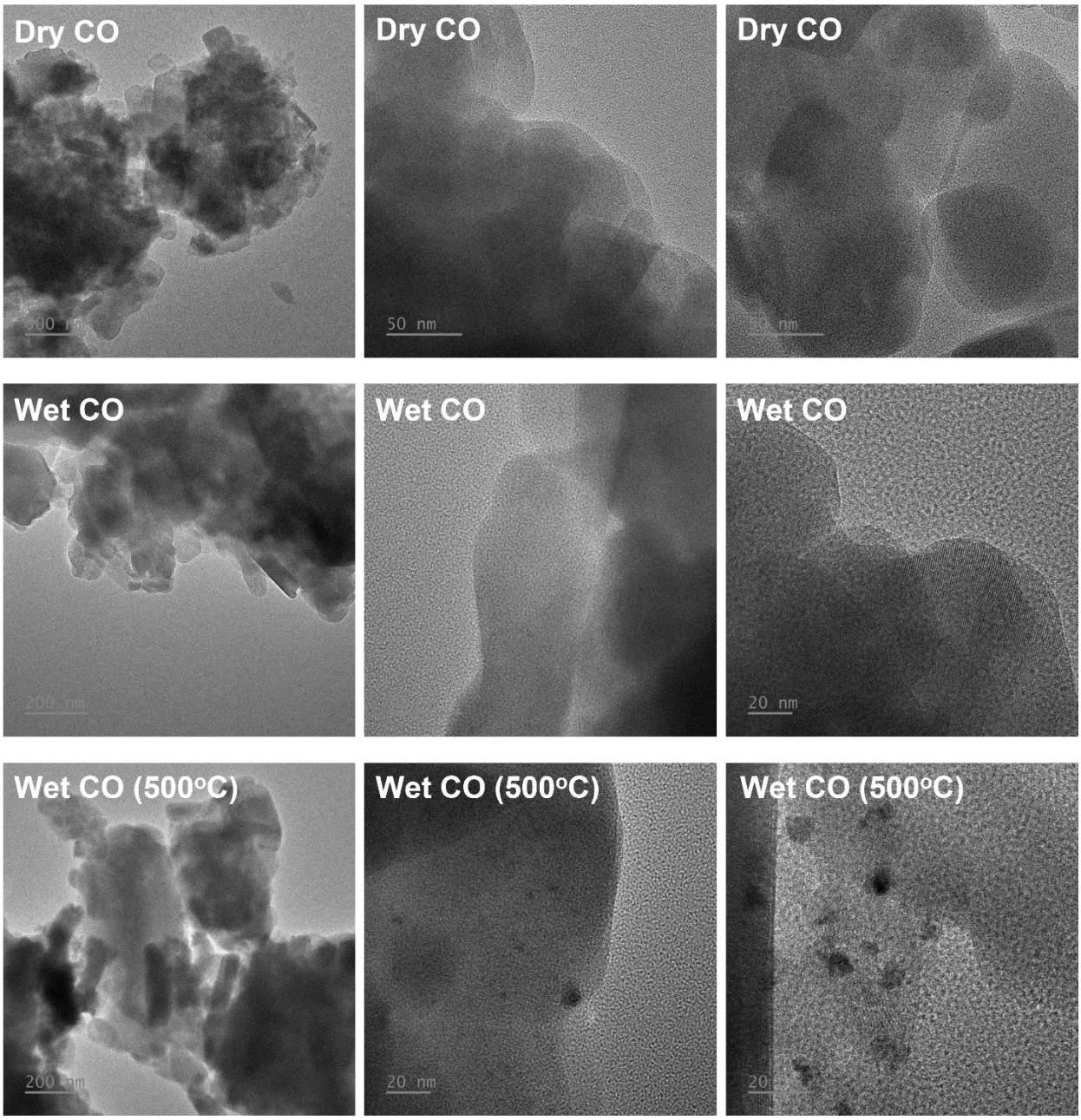

Figure S2. Extra transmission electron microscopy (TEM) results on Pd/FER treated under dry and wet CO (100 and 500 °C).

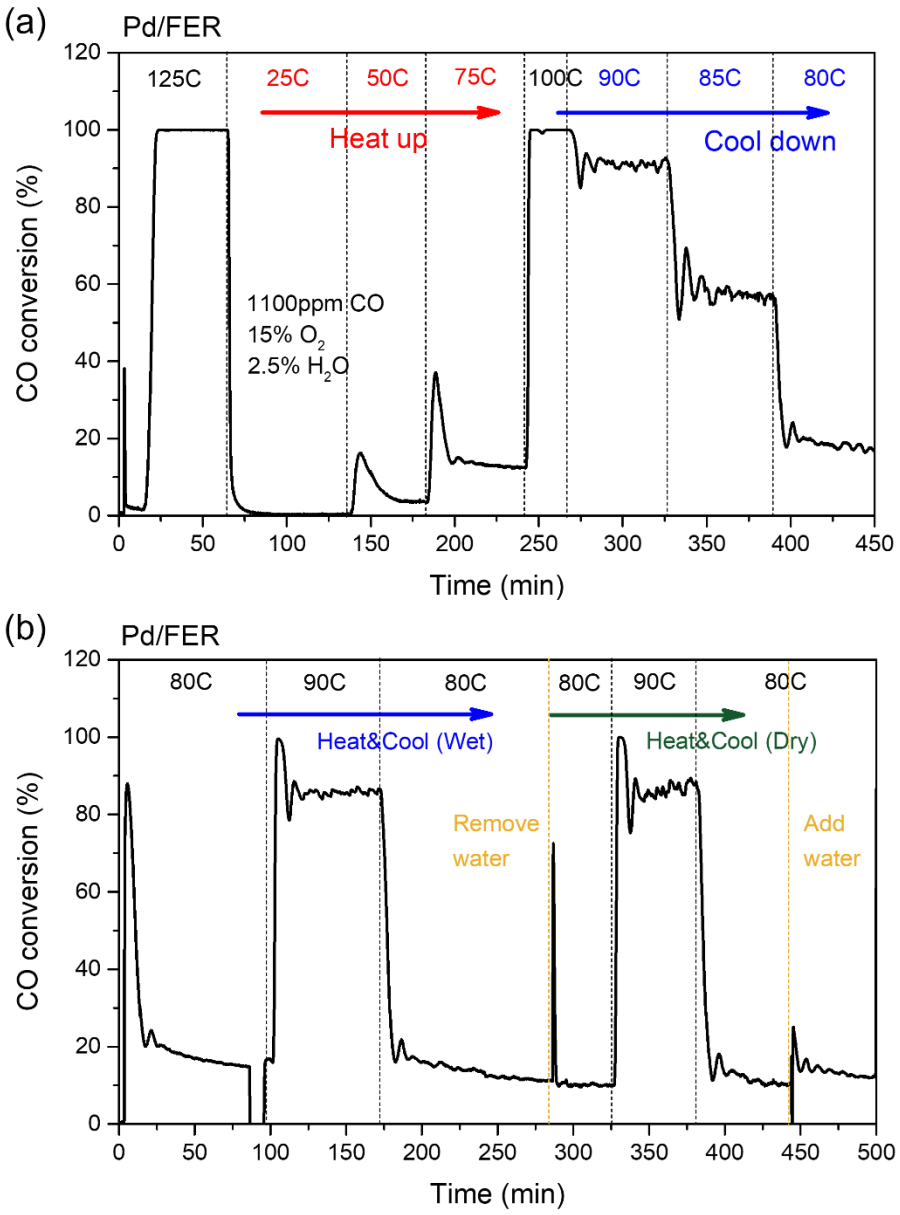

Figure S3. (a) Effect of temperature and (b) effect of water on catalytic CO oxidation over wet CO treated (125 °C, 30min) Pd/FER catalyst. The feed gas contains 1100 ppm CO and 15% O_2 balance with N_2 (GHSV: 225,000 mL·g^{-1}·h^{-1}).

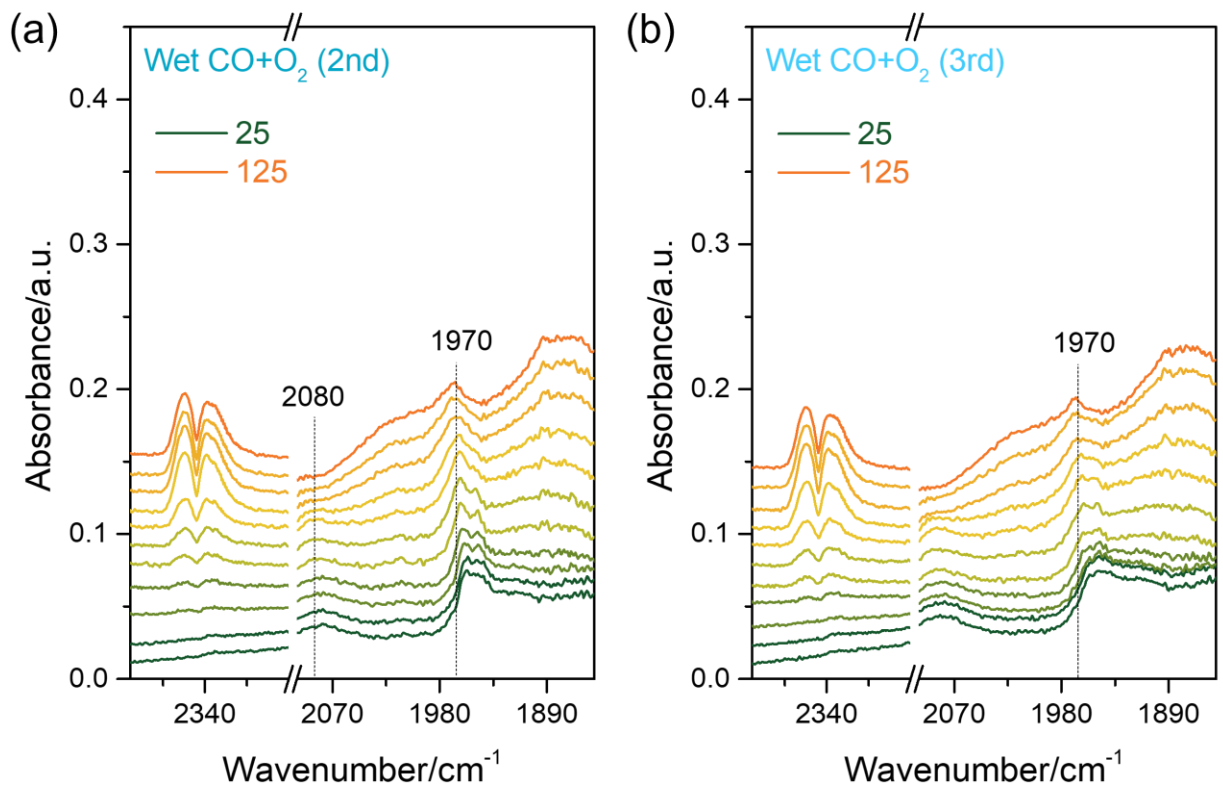

Figure S4. *In situ* DRIFTS spectra over Pd/FER during 2nd and 3rd wet CO oxidation from 25 to 125 °C (per 10°C, as in Figure 2). These experiments were conducted after conducting 1st CO oxidation in Figure 2b.

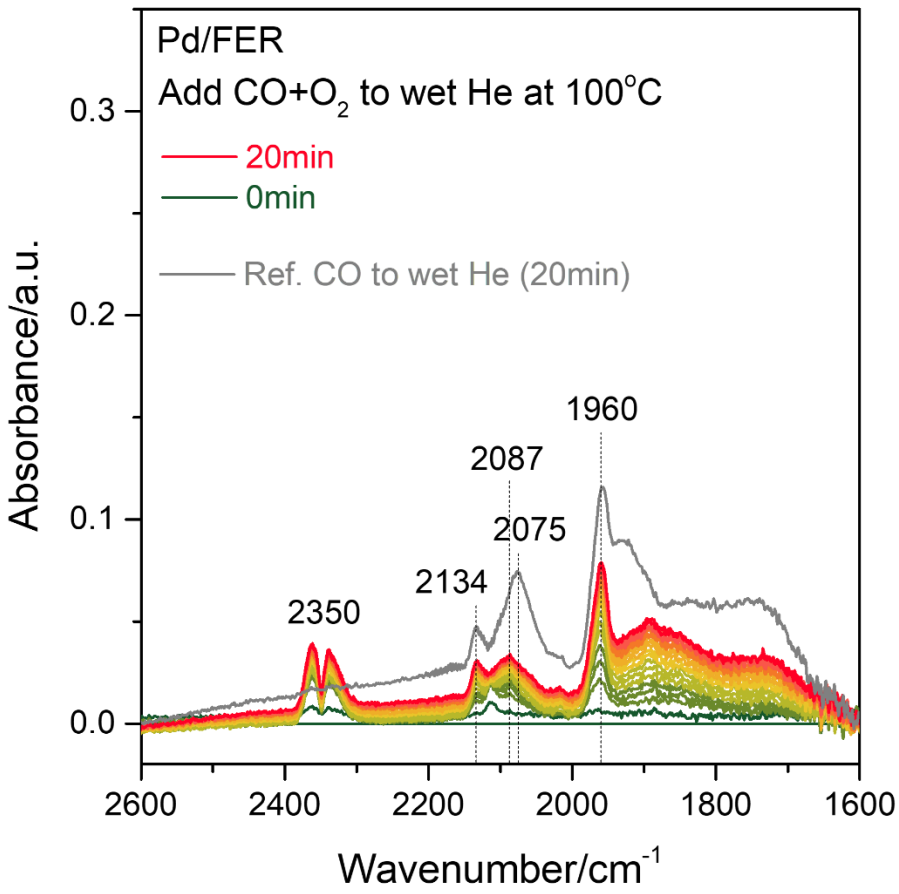

Figure S5. Series of DRIFTS spectra (per 1 min) obtained at 100 °C while flowing 800 ppm CO+15% O_2+2.8% H_2O/He on hydrated Pd/FER.

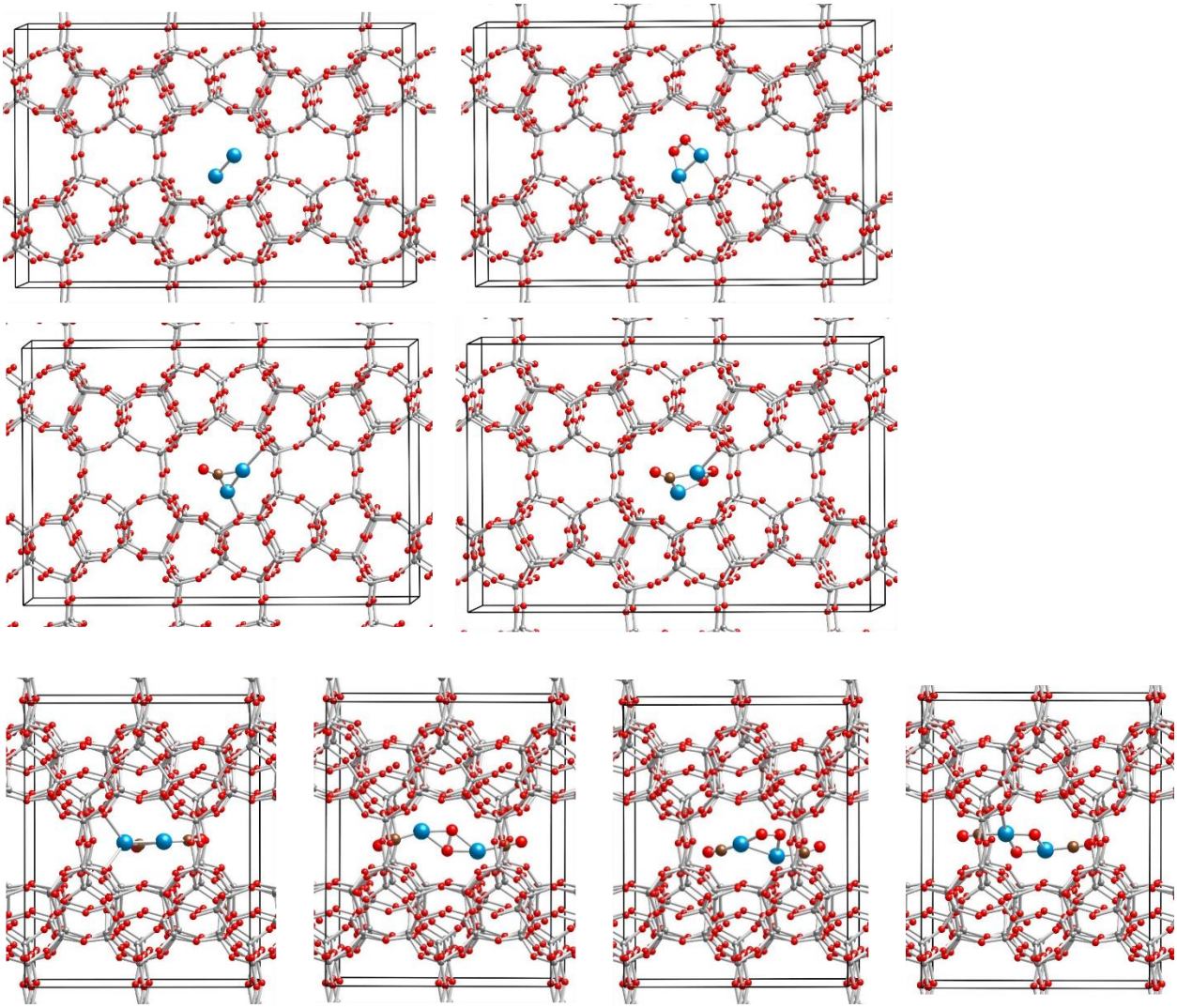

Figure S6. Left to right, top to bottom – optimized models of Pd_2/FER, $Pd_2(O_2)$/FER, $Pd_2(CO)$/FER, $Pd_2(CO)(O_2)$/FER, $Pd_2(CO)_2$/FER, $Pd_2(CO)_2(O_2)$/FER_1, $Pd_2(CO)_2(O_2)$/FER_2 and $Pd_2(CO)_2(O)_2$/FER. Color coding: Si – gray; O – red; Pd – blue and C – brown. For visual clarity, the oxygen atoms from the CO molecules are represented with larger size and structures $Pd_2(CO)_2$/FER, $Pd_2(CO)_2(O_2)$/FER_1, $Pd_2(CO)_2(O_2)$/FER_2 and $Pd_2(CO)_2(O)_2$/ FER are rotated by 90º with respect to the others.

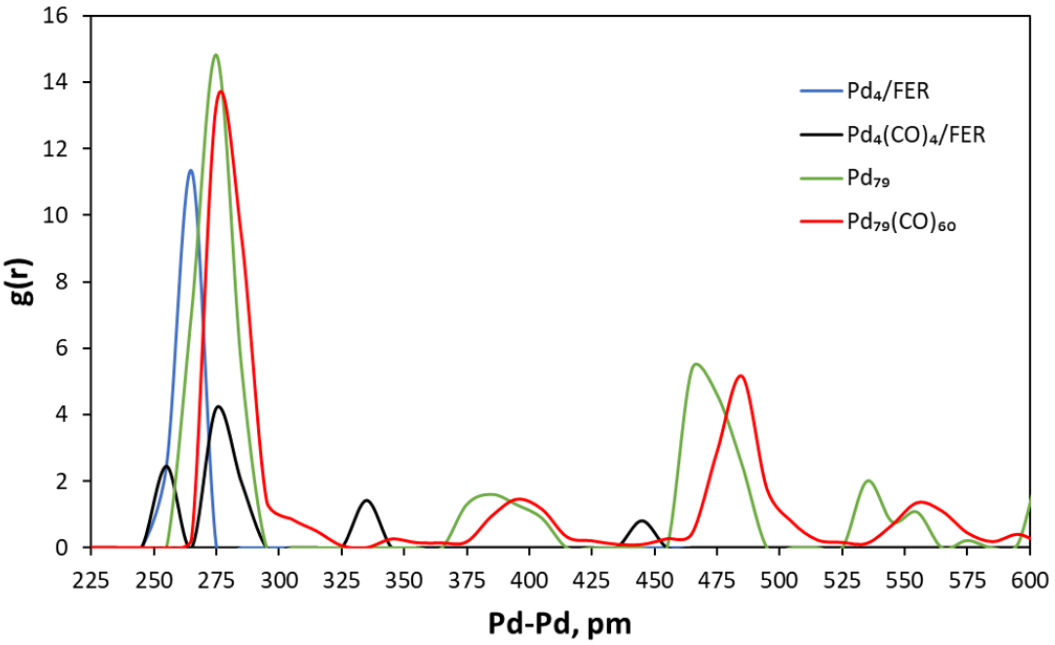

Figure S7. Radial distribution function for the Pd-Pd distances in the pristine and covered by CO Pd_4/FER and Pd_{79} nanoparticle models.